

MagicFace: Training-free Universal-Style Human Image Customized Synthesis

Yibin Wang^{1*}, Weizhong Zhang^{2*}, Cheng Jin^{1†}

¹School of Computer Science, Fudan University ²School of Data Science, Fudan University

yibinwang1121@163.com, weizhongzhang@fudan.edu.cn, jc@fudan.edu.cn

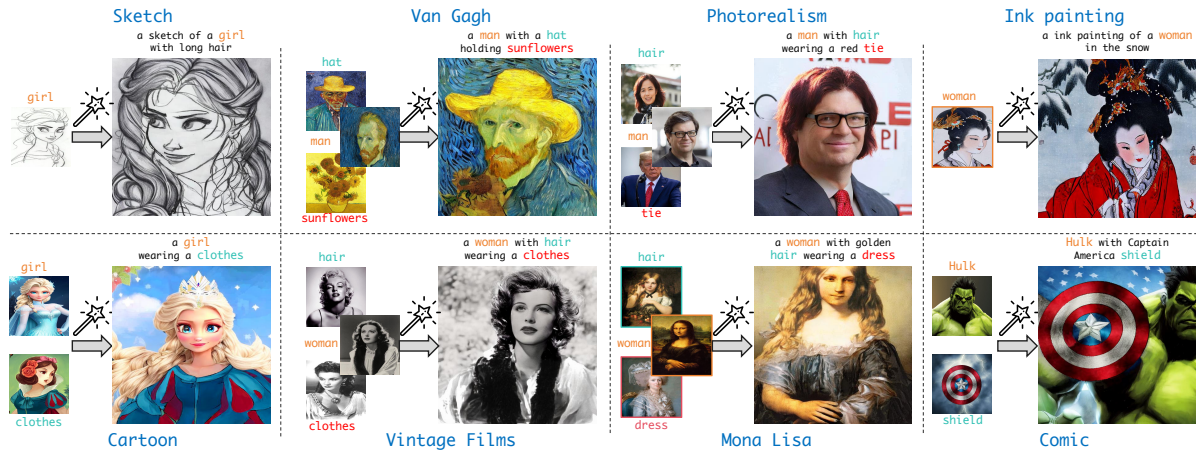


Figure 1. Results of single/multi-concept customization for humans across diverse styles. Each instance comprises two distinct inputs: a textual description, and a set of reference images. MagicFace is capable of generating high-fidelity images depicting the specific individual of any style with multiple given concepts in a training-free manner. Best viewed on screen.

Abstract

Current state-of-the-art methods for human image customized synthesis typically require tedious training on large-scale datasets. In such cases, they are prone to overfitting and struggle to personalize individuals of unseen styles. Moreover, these methods extensively focus on single-concept human image synthesis and lack the flexibility needed for customizing individuals with multiple given concepts, thereby impeding their broader practical application. To this end, we propose MagicFace, a novel training-free method for universal-style human image personalized synthesis, enabling multi-concept customization by accurately integrating reference concept features into their latent generated region at the pixel level. Specifically, MagicFace introduces a coarse-to-fine generation pipeline, involving two sequential stages: semantic layout construction and concept feature injection. This is achieved by our Reference-aware Self-Attention (RSA) and Region-grouped Blend Attention (RBA) mechanisms. In the first stage, RSA enables the latent image to query features from all reference concepts simultaneously, extracting the overall semantic understanding to facilitate

the initial semantic layout establishment. In the second stage, we employ an attention-based semantic segmentation method to pinpoint the latent generated regions of all concepts at each step. Following this, RBA divides the pixels of the latent image into semantic groups, with each group querying fine-grained features from the corresponding reference concept, which ensures precise attribute alignment and feature injection. Throughout the generation process, a weighted mask strategy is employed to ensure the model focuses more on the reference concepts. Extensive experiments demonstrate the superiority of MagicFace in both human-centric subject-to-image synthesis and multi-concept human image customization. It also can be applied to texture transfer, further enhancing its versatility and applicability. The project page is [here](#).

1. Introduction

Text-to-image generation has undergone remarkable advancements with the emergence of large-scale text-to-image diffusion models such as Stable Diffusion [23]. One of the most popular and challenging topics in these developments is

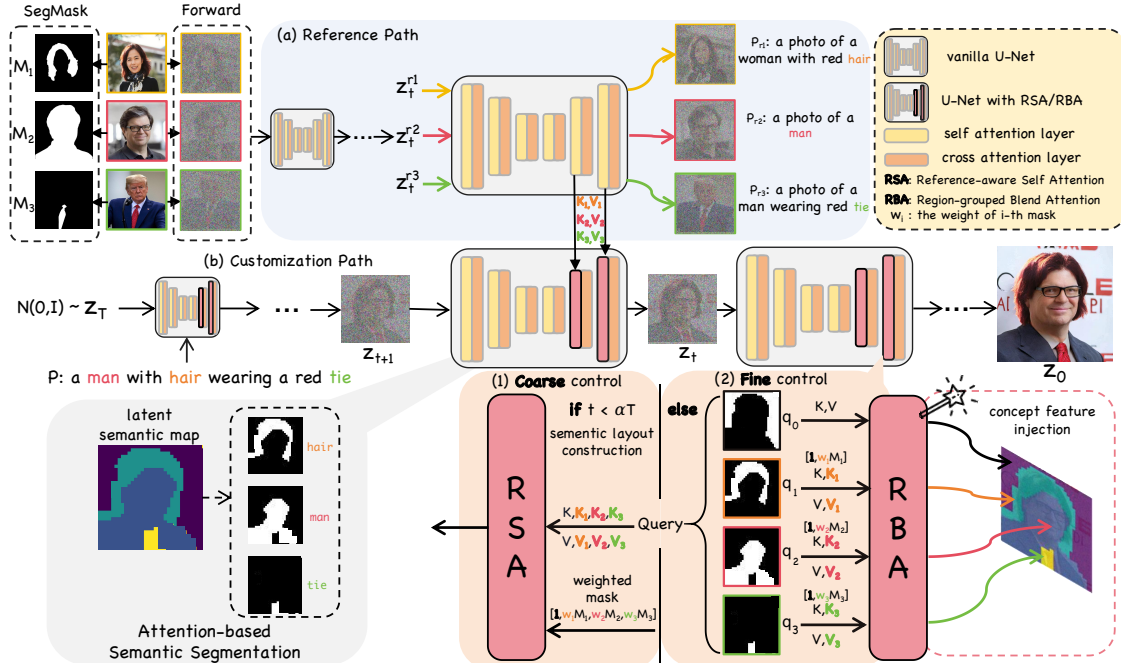


Figure 3. **Overview of our MagicFace.** Given reference images, their segmentation masks, and text prompts, we generate personalized image z_0 aligned to the target prompt P . The sampling pipeline consists of two paths: (a) the reference path and (b) the customization path. In (a), we first employ a diffusion forward process on the reference images. Then, the noised reference latents are input into vanilla U-Net. In (b), we first sample a Gaussian noise z_T and introduce a coarse-to-fine generation process involving two sequential stages: semantic layout construction and concept feature injection. At each step t , we pass latent z_t to our modified U-Net: (1) in the first stage, we employ RSA to integrate the features from the reference path to facilitate the initial semantic scene construction; (2) in the second stage, we first obtain the latent semantic map of z_t via attention-based segmentation method. Based on this, RBA divides the latent image and ensures fine-grained feature injection for each generated concept. A weighted mask strategy is adopted to ensure the model focuses more on given concepts.

RSA and RBA, ensures precise attribute alignment and feature injection for each concept.

- Our method can be applied to texture transfer, showcasing its versatility and applicability.

2. Related Work

Human image personalized generation is one of the most widely demanded and challenging directions in subject-driven image generation. The goal is to synthesize new images depicting specific individuals in novel scenes, styles, and actions. Current methods can be mainly divided into two categories: tuning-based customization and zero-shot customization.

Tuning-based Customization. Tuning-based methods rely on additional subject-specific optimization during test time. The pioneering work, Dreambooth [24], fine-tunes a text-to-image diffusion model using numerous reference images to bind a unique identifier to the given subject. A concurrent work, Textual Inversion [9] transforms subject images into a simple learnable text embedding to encode the subject’s identity. Following this, subsequent works such as NeTI [1] and XTI [31] introduce implicit time-aware representation and layer-wise learnable embedding respectively to

achieve better performance. Additionally, Tuning-Encoder [3] generates an initial set of latent codes using a pre-trained encoder and refines these codes with minimal fine-tuning iterations to better preserve subject identities. Despite their effectiveness, these methods always encounter inefficiency due to their demand of considerable time and computing resources for fine-tuning in the test time.

Zero-shot Customization. Zero-shot methods attempt to perform customization using a single image with a single forward pass, significantly accelerating the personalization process. For example, ELITE [35] and InstantBooth [27] achieve this by utilizing a global mapping network to encode reference images into word embeddings and a local mapping network to inject reference image patch features into cross-attention layers. Fastcomposer [36] and PhotoMaker [17] extract identity-centric embeddings by fine-tuning the image encoder and merging the class and image embeddings. Face-Diffuser [34] reveals the training imbalance and quality compromise issues in these methods and addresses them by proposing a novel collaborative generation pipeline. InstantID [33] proposes an IdentityNet to steer the generation by integrating facial and landmark images with textual prompts. FlashFace [39] encodes the reference image into a series

of feature maps to maintain more details. Despite their impressive results, these methods struggle to personalize individuals of unseen styles limited by their training datasets. Besides, they only focus on single-concept human personalization and fail to deal with complex scenarios involving multiple concepts.

Multi-concept Image Customization. Different from these works, recent studies focus on multi-subject customization. Custom Diffusion [16] achieves this by closed-form constrained optimization for multiple concepts. Perfusion [30] proposes a dynamic rank-1 update strategy to maintain high visual fidelity. FreeCustom [7] proposes a multi-reference self-attention mechanism, allowing the latent image to interact with the input concepts. ClassDiffusion [13] leverages a semantic preservation loss to explicitly regulate the concept space when learning a new concept. Despite their effectiveness on general objects with coarse-grained textures, these approaches fall short in human customization due to the nuanced semantics and higher level of detail and fidelity required for facial identity.

3. MagicFace

3.1. Overview

We present an overview of our proposed MagicFace in Fig. 3. Our goal is to achieve high-fidelity human image personalization, enabling multi-concept customization for humans across various styles in a training-free manner. To accomplish this, we propose a coarse-to-fine generation pipeline, incorporating our Reference-aware Self-Attention (RSA) and Region-grouped Blend Attention (RBA) mechanisms. Specifically, our sampling process involves two sequential stages with a total of T denoising steps.

In the first stage, we employ RSA to extract the overall semantic understanding from all given concepts, facilitating the initial semantic scene construction.

In the second stage, a latent semantic map is first derived to pinpoint the generated regions of all concepts at each step. We then utilize RBA to accurately inject features of reference concepts into their corresponding regions, ensuring the generated concepts closely resemble the reference images.

To emphasize the model’s attention to the reference concepts, a weighted mask strategy is implemented during customized synthesis.

3.1.1 Vanilla Self-attention in Diffusion Model

In this work, we adopt pre-trained Stable Diffusion (SD) [22] as our base model, utilizing its U-Net ϵ_θ as the denoiser. The original SD U-Net is composed of 16 layers with each layer including a residual block, a self-attention module, and a cross-attention module. The self-attention (SA) layer in U-Net is crucial for establishing the layout and detailing the

content, which can be formulated as

$$\text{SA}(\mathbf{Q}, \mathbf{K}, \mathbf{V}) = \text{Softmax}\left(\frac{\mathbf{Q}\mathbf{K}^\top}{\sqrt{d}}\right)\mathbf{V}, \quad (1)$$

where \mathbf{Q} , \mathbf{K} , and \mathbf{V} are the query, key, and value projected from the latent image feature using different linear mappings with the dimension d .

3.1.2 Dual-path Guided Synthesis

As illustrated in Fig. 3, the overall inference pipeline involves two paths: reference path and customization path, which will be elaborated in the following.

Reference Path. For each concept image in the reference path, we first apply a diffusion forward process [11] to compute the noised reference latent \mathbf{z}'_T . At each step t , we input \mathbf{z}'_t and its text prompt into the U-Net ϵ_θ . In the self-attention layer l and time step t , we extract the $\mathbf{K}_{i,l,t}$ and $\mathbf{V}_{i,l,t}$ of i -th concept to guide the synthesis in the customization path.

Customization Path. This path starts by sampling the latent \mathbf{z}_T from the Gaussian distribution. Then, we modify the vanilla self-attention module in SD U-Net, extending it into our RSA/RBA. At each step t , we pass the latent \mathbf{z}_t and target prompt P into modified U-Net ϵ_θ^* , integrating concept features from $\mathbf{K}_{i,l,t}$ and $\mathbf{V}_{i,l,t}$ derived in reference path. The final denoised result is the ultimate synthesized image.

3.2. Coarse-to-Fine Generation Process

MagicFace synthesizes images by progressing from coarse-grained semantic scene construction with αT steps to fine-grained feature injection with $T(1-\alpha)$ steps in an evolving scheme. In the latter stage, we employ an attention-based semantic segmentation method, which paves the way for precise feature injection. We will delve into the details of each stage in the following.

3.2.1 Semantic Scene Construction

Reference-aware Self-Attention. RSA enables the latent image to query features from all reference concepts simultaneously to integrate coarse-grained semantic information for initial semantic scene construction. Specifically, in each self-attention layer l and time step t , the query, key, and value feature from \mathbf{z}_t are $\mathbf{Q}_{l,t}$, $\mathbf{K}_{l,t}$ and $\mathbf{V}_{l,t}$. We then concatenate $\mathbf{K}_{l,t}$ and $\mathbf{V}_{l,t}$ with injected key and value features of N concepts from reference path, resulting in $\hat{\mathbf{K}} = [\mathbf{K}, \mathbf{K}_1, \mathbf{K}_2, \dots, \mathbf{K}_N]$ and $\hat{\mathbf{V}} = [\mathbf{V}, \mathbf{V}_1, \mathbf{V}_2, \dots, \mathbf{V}_N]$ where we omit l, t for brevity. However, we aim to query features exclusively from the concept region, as irrelevant background information in the reference image may distract the model and reduce its effectiveness. To address this issue, we rectify the model’s attention by introducing the segmentation mask \mathbf{M}_i of each reference

concept and concatenate them with an all-ones matrix to obtain $\mathbf{M} = [\mathbf{1}, w_1\mathbf{M}_1, w_2\mathbf{M}_2, \dots, w_N\mathbf{M}_N]$ where w_i represents the scaling weight for each mask (elaborated in Sec. 3.2.4). Ultimately, the RSA can be formulated as follows:

$$\text{RSA}(\mathbf{Q}, \hat{\mathbf{K}}, \hat{\mathbf{V}}, \mathbf{M}) = \text{Softmax}\left(\frac{\mathbf{M} \odot \mathbf{Q}\hat{\mathbf{K}}^T}{\sqrt{d}}\right)\hat{\mathbf{V}}. \quad (2)$$

Here, \odot denotes the Hadamard product. This process ensures the generated image effectively interacts with the overall semantic information from the reference images while filtering out unrelated noise.

3.2.2 Latent Semantic Map Generation

To ensure precise feature injection for each concept at the pixel level, we need to identify their latent generated region. However, this task is challenging because the latent image at each step is not accessible during the generation process. Fortunately, the attention layers in the U-Net contain rich semantic information, which can be utilized to identify semantic units efficiently [5]. Therefore, we compute the latent semantic map based on attention maps, involving two sequential steps: cross-attention-based semantic segmentation and self-attention-based segmentation completion.

Attention Maps Generation. In the attention layer l and time step t , a self-attention map \mathbf{S}_t^l and a cross-attention map \mathbf{C}_t^l are calculated over linear projections of the intermediate image spatial feature \mathbf{z}_t^l or text embedding \mathbf{e} ,

$$\mathbf{S}_t^l = \text{Softmax}\left(\frac{\mathbf{Q}_s(\mathbf{z}_t^l)\mathbf{K}_s(\mathbf{z}_t^l)^T}{\sqrt{d}}\right), \quad (3)$$

$$\mathbf{C}_t^l = \text{Softmax}\left(\frac{\mathbf{Q}_c(\mathbf{z}_t^l)\mathbf{K}_c(\mathbf{e})^T}{\sqrt{d}}\right), \quad (4)$$

where $\mathbf{Q}_*(\cdot)$ and $\mathbf{K}_*(\cdot)$ are linear projections with the dimension d . Though self-attention modules are modified in our framework, we still compute the original self-attention maps for latent semantic map generation at each step.

Semantic Segmentation. Cross-attention maps contain the similarity values between image patch s and text token P_i . Therefore, in each row of \mathbf{C}_t^l , a higher probability $\mathbf{C}_t^l[s, i]$ indicates a closer relationship between s and P_i . Based on this, we segment the \mathbf{z}_t^l as the set of regions masked by $[\mathbf{m}_1, \mathbf{m}_2, \dots, \mathbf{m}_K]$, with K denotes the number of tokens and $\mathbf{m}_i \in \{0, 1\}$ indicate the latent semantic region of token P_i .

Specifically, we first upsample all cross-attention maps \mathbf{C}_t^l to the same size, then average and renormalize them along the spatial dimension to obtain the final cross-attention map, formulated as $\mathbf{C}_t = \Phi(\mathbf{C}_t^l)$. This map estimates the likelihood of assigning patch s for the token P_i . Ultimately, the argmax operation is applied to the token dimension to determine the activation of each patch:

$$i_s = \arg \max_i \mathbf{C}_t[s, i]. \quad (5)$$

Along this line, we compute \mathbf{m}_i by setting the element in the patch set $\{s : i_s = i\}$ as 1, and others to 0. Note that we only need the semantic masks of N reference concepts for feature injection. Hence, we retain the masks of concept-specific tokens and merge the remaining ones into a new mask \mathbf{m}_0 indicating the background region, yielding $\mathcal{M} = [\mathbf{m}_0, \mathbf{m}_1, \mathbf{m}_2, \dots, \mathbf{m}_N]$.

Visualization. The first row in Fig. 4 demonstrates the result of the aforementioned semantic segmentation results. The semantic maps effectively identify the rough locations of the generated concepts. However, they often exhibit unclear boundaries and may contain internal gaps, leading to problematic results. To address this issue, we refine and complete the semantic map using self-attention maps [32], as detailed in the following section.

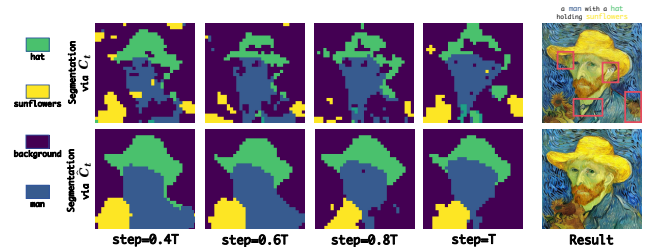


Figure 4. **Visualization of semantic maps derived by \mathbf{C}_t and $\hat{\mathbf{C}}_t$.** Regions labeled with different colors correspond to different concepts. Problematic regions are highlighted using the outline.

Segmentation Completion. Self-attention maps \mathbf{S}_t^l estimate the correlation between image patches, thereby can be used to refine incomplete activation regions in cross-attention maps via transmitting semantic information across patches. This approach is analogous to the feature propagation in spectral graph convolution [14], as self-attention maps can be viewed as transition matrices where each element is nonnegative and the sum of each row sums to 1. Consequently, we refine the cross-attention maps \mathbf{C}_t^l by multiplying them with their corresponding self-attention maps, yielding $\hat{\mathbf{C}}_t^l = \mathbf{S}_t^l \mathbf{C}_t^l$. Based on this, the refined final cross-attention map denoted as $\hat{\mathbf{C}}_t = \Phi(\hat{\mathbf{C}}_t^l)$, is then used in Eq. (5) to derive refined latent semantic masks \mathcal{M} .

Visualization. The last row in Fig. 4 demonstrates the effectiveness of the refinement where the resulting segmentation maps indicate clearer object boundaries and fewer internal holes.

3.2.3 Concept Feature Injection

Region-grouped Blend Attention. With the latent semantic masks \mathcal{M} , RBA divides the latent image into concept groups, enabling each generated concept to query fine-grained features from the corresponding reference image. Specifically, at each self-attention layer l and time step t , the query, key, and value feature from \mathbf{z}_t are \mathbf{Q} , \mathbf{K} , and \mathbf{V} . We omit l, t for

brevity. Next, we segment the Q into groups $[q_0, q_1, \dots, q_N]$ based on \mathcal{M} . For each group q_i where $i > 0$, we concatenate K and V with their corresponding injected key and value features from reference path, resulting in $\tilde{K}_i = [K, K_i]$ and $\tilde{V}_i = [V, V_i]$. For the feature group q_0 corresponding to the background, we have $\tilde{K}_0 = K$ and $\tilde{V}_0 = V$. Based on this, we individually compute the region-grouped attention output x_i as:

$$x_i = \text{Softmax}\left(\frac{\tilde{M}_i \odot q_i \tilde{K}_i^T}{\sqrt{d}}\right) \tilde{V}_i, \quad (6)$$

where $\tilde{M}_i = [\mathbf{1}, w_i M_i]$ for $i > 0$, and \tilde{M}_0 is an all-ones matrix. Finally, we blend the outputs $[x_0, x_1, \dots, x_N]$ into a single output by putting the pixels from each output into their corresponding positions based on \mathcal{M} . This process effectively ensures precise attribute alignment and feature injection for each generated concept.

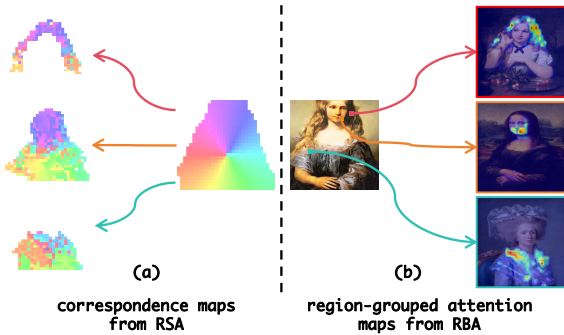


Figure 5. **Correspondence maps and region-grouped attention maps visualization.** In (a), features with the highest similarity between the generated subject and the reference concepts are marked with the same color. (b) the results of features in colored boxes querying their reference concept keys.

3.2.4 Weighted Mask Strategy

Despite segmentation masks of reference concepts helping to mitigate the disturbance of unrelated background information, the model still struggles to accurately capture the unique attributes of the target concept, particularly when it comes to preserving human identity. Therefore, we introduce a scaling factor w_i to each mask M_i during the RSA and RBA processes, aiming to enhance the model’s focus on the desired concept features. The effectiveness of this strategy is examined in Fig. 6 and further discussed in Sec. 4.3.

4. Experiment

4.1. Implementation details

Datasets.

Subject-to-Image Generation. The evaluation dataset consists of 35 human identities (IDs): 24 from previous work



Figure 6. **Visualized results under different weight settings w .** Problematic regions are highlighted using the outline.

[18, 34] and 11 newly collected. Each ID includes 3 reference images and 1 target image. We also collect 30 prompts covering expressions, attributes, actions, etc. from [17].

Multi-concept Customization. The evaluation dataset consists of 30 sample images collected from the previous works [1, 7, 34] and the Internet. Each image includes an ID and 2-3 reference accessories. The segmentation masks of all reference concepts are generated by segment-anything [15]. **Configurations.** Our method is training-free and employs Stable-Diffusion v1.5 as the base model for evaluation using an NVIDIA 3090 GPU. We use 50 steps of the DDIM sampler [29]. The scale of classifier-free guidance is set to 7.5. The mask weight w is set to 3 for each concept. We only modify the self-attention module in blocks 5 and 6 of the U-Net. The hyperparameter α is set to 0.4.

Evaluation. We use CLIP-I [8] and DINO [4] metrics to measure image fidelity, and CLIP-T [21] to assess prompt consistency. Face similarity is calculated by detecting facial regions with MTCNN [38] and then computing pairwise ID similarity using FaceNet [26].

4.2. Results

For a comprehensive evaluation, we compare our method with baselines in human-centric subject-to-image generation and multi-concept customization domains. The quantitative compared results are shown in Tab. 1. Notably, our method significantly improves the CLIP-T metric compared to subject-to-image generation baselines. This improvement is expected, as these methods, trained on large-scale datasets, tend to overfit and consequently struggle with generating unseen semantic scenes. For multi-concept customization, all competing methods exhibit poor performance on the face similarity metric, highlighting their significant challenges in preserving facial identity. The qualitative compared results are provided in Fig. 2 and Fig. 7.

4.3. Ablation Studies

Visualization of RSA and RBA. We visualize the correspondence between each feature in the generated image and the concept image based on their attention maps in RSA, as well as the attention maps derived by selected image patches

Table 1. Quantitative comparison against baselines.

Methods	Subject-to-Image Generation				Methods	Multi-Concept Customization			
	CLIP-T	CLIP-I	DINO	Face-sim.		CLIP-T	CLIP-I	DINO	Face-sim.
'23 Fastcomposer (SD1.5) [36]	29.1	67.4	42.3	59.8	'23 Perfusion (SD1.5) [30]	23.2	41.6	30.2	25.7
'23 PhotoMaker (SDXL) [17]	28.5	71.9	53.5	63.2	'23 CustomDiffusion (SD1.5) [16]	28.4	39.3	31.4	27.2
'24 InstantID (SDXL) [33]	29.6	69.2	51.8	61.7	'24 FreeCustom (SD1.5) [7]	31.4	55.4	42.1	43.2
'24 FlashFace (SD1.5) [39]	30.4	75.1	52.7	64.9	'24 ClassDiffuion (SD1.5) [13]	32.8	51.2	38.5	35.4
MagicFace (SD1.5)	33.6	76.5	55.2	66.1	MagicFace (SD1.5)	34.2	59.4	45.3	51.8



Figure 7. Qualitative comparative results on multi-concept customization.

querying their corresponding reference concepts in RBA. As shown in Fig. 5, (a) the similar regions in the generated and reference images indicate higher correlation, and (b) these patches precisely capture features from their reference concepts.

Choice of weights w . We explore the impacts of different weight settings in Fig. 6. We observe that the results improved significantly when adopting the weighted masks. Although higher weights for each concept lead to more faithful generation, as shown in the first row, excessively high weights can cause coherence issues for easily generated objects such as the tie in this case. Therefore, balancing the weights is crucial to ensure that the generated concepts are both accurate and harmoniously integrated within the scene.

Choice of the hyperparameter α . In this work, RSA handles semantic layout construction for αT steps, and RBA takes over for concept feature injection in the remaining steps. We analyze the optimal value of α in Fig. 8. When $\alpha = 0$, the generated concepts differ significantly from the reference concepts on shape, such as facial form, due to the absence of RSA. Conversely, when $\alpha = 1$, which excludes RBA, the results struggle with identity preservation. These observations highlight the effectiveness of both RSA and RBA. Finally, we find that $\alpha = 0.4$ achieves the best balance between semantic layout and identity preservation.

4.4. Applications

Universal-style human customization. MagicFace excels in personalizing humans across diverse styles as shown in Fig. 1. Unlike existing methods, which are limited to the photorealistic style due to their training datasets, MagicFace

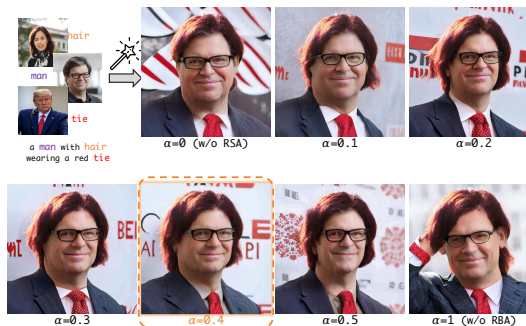


Figure 8. Hyperparameter analysis of α .

is training-free and effectively customizes humans of different styles by accurately embedding reference image features into the generated concept.

Texture transfer. MagicFace is also highly effective for texture transfer, as demonstrated in Fig. 9. It seamlessly transfers the appearance of input images into generated objects by precisely injecting texture features, further showcasing its versatility and effectiveness.

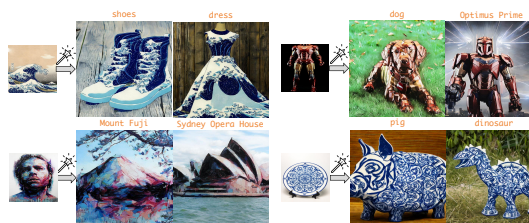


Figure 9. **Texture transfer.** Our method can inject the texture or materials of input images into generated objects.

5. Conclusion

In this paper, we propose MagicFace, the first method for universal-style human image personalized generation that enables multi-concept customization in a training-free manner. MagicFace features a coarse-to-fine generation pipeline with two sequential stages: RSA for establishing the initial semantic layout by extracting overall semantic understanding from all reference images, and RBA for precise feature injection by integrating fine-grained features from reference concepts into their respective latent generated regions. Extensive experiments highlight its superiority both qualitatively and quantitatively.

References

- [1] Yuval Alaluf, Elad Richardson, Gal Metzer, and Daniel Cohen-Or. A neural space-time representation for text-to-image personalization. *ACM Transactions on Graphics*, 42(6):1–10, 2023. [3](#), [6](#)
- [2] Moab Arar, Rinon Gal, Yuval Atzmon, Gal Chechik, Daniel Cohen-Or, Ariel Shamir, and Amit H. Bermano. Domain-agnostic tuning-encoder for fast personalization of text-to-image models. In *SIGGRAPH Asia*, pages 1–10, 2023. [2](#)
- [3] Moab Arar, Rinon Gal, Yuval Atzmon, Gal Chechik, Daniel Cohen-Or, Ariel Shamir, and Amit H. Bermano. Domain-agnostic tuning-encoder for fast personalization of text-to-image models. In *SIGGRAPH Asia*, pages 1–10, 2023. [3](#)
- [4] Mathilde Caron, Hugo Touvron, Ishan Misra, Hervé Jégou, Julien Mairal, Piotr Bojanowski, and Armand Joulin. Emerging properties in self-supervised vision transformers. In *ICCV*, pages 9650–9660, 2021. [6](#)
- [5] Hila Chefer, Yuval Alaluf, Yael Vinker, Lior Wolf, and Daniel Cohen-Or. Attend-and-excite: Attention-based semantic guidance for text-to-image diffusion models. *ACM Transactions on Graphics*, 42(4):1–10, 2023. [5](#)
- [6] Li Chen, Mengyi Zhao, Yiheng Liu, Mingxu Ding, Yangyang Song, Shizun Wang, Xu Wang, Hao Yang, Jing Liu, Kang Du, et al. Photoverse: Tuning-free image customization with text-to-image diffusion models. *arXiv preprint arXiv:2309.05793*, 2023. [2](#)
- [7] Ganggui Ding, Canyu Zhao, Wen Wang, Zhen Yang, Zide Liu, Hao Chen, and Chunhua Shen. Freecustom: Tuning-free customized image generation for multi-concept composition. In *CVPR*, pages 9089–9098, 2024. [2](#), [4](#), [6](#), [7](#)
- [8] Rinon Gal, Yuval Alaluf, Yuval Atzmon, Or Patashnik, Amit H Bermano, Gal Chechik, and Daniel Cohen-Or. An image is worth one word: Personalizing text-to-image generation using textual inversion. *arXiv preprint arXiv:2208.01618*, 2022. [6](#)
- [9] Rinon Gal, Yuval Alaluf, Yuval Atzmon, Or Patashnik, Amit H Bermano, Gal Chechik, and Daniel Cohen-Or. An image is worth one word: Personalizing text-to-image generation using textual inversion. In *ICLR*, 2023. [3](#), [10](#)
- [10] Yue Han, Junwei Zhu, Keke He, Xu Chen, Yanhao Ge, Wei Li, Xiangtai Li, Jiangning Zhang, Chengjie Wang, and Yong Liu. Face adapter for pre-trained diffusion models with fine-grained id and attribute control. *arXiv preprint arXiv:2405.12970*, 2024. [2](#)
- [11] Jonathan Ho, Ajay Jain, and Pieter Abbeel. Denoising diffusion probabilistic models. In *NeurIPS*, pages 6840–6851, 2020. [4](#)
- [12] Edward J Hu, Yelong Shen, Phillip Wallis, Zeyuan Allen-Zhu, Yuanzhi Li, Shean Wang, Lu Wang, and Weizhu Chen. Lora: Low-rank adaptation of large language models. In *ICLR*, 2022. [2](#)
- [13] Jiannan Huang, Jun Hao Liew, Hanshu Yan, Yuyang Yin, Yao Zhao, and Yunchao Wei. Classdiffusion: More aligned personalization tuning with explicit class guidance. *arXiv preprint arXiv:2405.17532*, 2024. [4](#), [7](#)
- [14] Thomas N Kipf and Max Welling. Semi-supervised classification with graph convolutional networks. *arXiv preprint arXiv:1609.02907*, 2016. [5](#)
- [15] Alexander Kirillov, Eric Mintun, Nikhila Ravi, Hanzi Mao, Chloe Rolland, Laura Gustafson, Tete Xiao, Spencer Whitehead, Alexander C Berg, Wan-Yen Lo, et al. Segment anything. In *ICCV*, pages 4015–4026, 2023. [6](#)
- [16] Nupur Kumari, Bingliang Zhang, Richard Zhang, Eli Shechtman, and Jun-Yan Zhu. Multi-concept customization of text-to-image diffusion. In *CVPR*, pages 1931–1941, 2023. [2](#), [4](#), [7](#)
- [17] Zhen Li, Mingdeng Cao, Xintao Wang, Zhongang Qi, Ming-Ming Cheng, and Ying Shan. Photomaker: Customizing realistic human photos via stacked id embedding. In *CVPR*, pages 8640–8650, 2024. [2](#), [3](#), [6](#), [7](#)
- [18] Yotam Nitzan, Kfir Aberman, Qiuwei He, Orly Liba, Michal Yarom, Yossi Gandelsman, Inbar Mosseri, Yael Pritch, and Daniel Cohen-Or. Mystyle: A personalized generative prior. *ACM Transactions on Graphics*, 41(6):1–10, 2022. [6](#)
- [19] Marianna Ohanian, Hayk Manukyan, Zhangyang Wang, Shant Navasardyan, and Humphrey Shi. Zero-painter: Training-free layout control for text-to-image synthesis. In *CVPR*, pages 8764–8774, 2024. [2](#)
- [20] Senthil Purushwalkam, Akash Gokul, Shafiq Joty, and Nikhil Naik. Bootpig: Bootstrapping zero-shot personalized image generation capabilities in pretrained diffusion models. *arXiv preprint arXiv:2401.13974*, 2024. [2](#)
- [21] Alec Radford, Jong Wook Kim, Chris Hallacy, Aditya Ramesh, Gabriel Goh, Sandhini Agarwal, Girish Sastry, Amanda Askell, Pamela Mishkin, Jack Clark, et al. Learning transferable visual models from natural language supervision. In *ICML*, pages 8748–8763. PMLR, 2021. [6](#)
- [22] Robin Rombach, Andreas Blattmann, Dominik Lorenz, Patrick Esser, and Björn Ommer. High-resolution image synthesis with latent diffusion models. In *CVPR*, pages 10684–10695, 2022. [4](#)
- [23] Robin Rombach, Andreas Blattmann, Dominik Lorenz, Patrick Esser, and Björn Ommer. High-resolution image synthesis with latent diffusion models. In *CVPR*, pages 10684–10695, 2022. [1](#)
- [24] Nataniel Ruiz, Yuanzhen Li, Varun Jampani, Yael Pritch, Michael Rubinstein, and Kfir Aberman. Dreambooth: Fine tuning text-to-image diffusion models for subject-driven generation. In *CVPR*, pages 22500–22510, 2023. [2](#), [3](#), [10](#)
- [25] Nataniel Ruiz, Yuanzhen Li, Varun Jampani, Wei Wei, Tingbo Hou, Yael Pritch, Neal Wadhwa, Michael Rubinstein, and Kfir Aberman. Hyperdreambooth: Hypernetworks for fast personalization of text-to-image models. In *CVPR*, pages 6527–6536, 2024. [2](#)
- [26] Florian Schroff, Dmitry Kalenichenko, and James Philbin. Facenet: A unified embedding for face recognition and clustering. In *CVPR*, pages 815–823, 2015. [6](#)
- [27] Jing Shi, Wei Xiong, Zhe Lin, and Hyun Joon Jung. Instantbooth: Personalized text-to-image generation without test-time finetuning. *arXiv preprint arXiv:2304.03411*, 2023. [3](#)
- [28] Chenyang Si, Ziqi Huang, Yuming Jiang, and Ziwei Liu. Freeu: Free lunch in diffusion u-net. In *CVPR*, pages 4733–4743, 2024. [2](#)

- [29] Jiaming Song, Chenlin Meng, and Stefano Ermon. Denoising diffusion implicit models. *arXiv preprint arXiv:2010.02502*, 2020. [6](#)
- [30] Yoad Tewel, Rinon Gal, Gal Chechik, and Yuval Atzmon. Key-locked rank one editing for text-to-image personalization. In *ACM SIGGRAPH*, pages 1–11, 2023. [2](#), [4](#), [7](#)
- [31] Andrey Voynov, Qinghao Chu, Daniel Cohen-Or, and Kfir Aberman. p+: Extended textual conditioning in text-to-image generation. *arXiv preprint arXiv:2303.09522*, 2023. [3](#)
- [32] Jinglong Wang, Xiawei Li, Jing Zhang, Qingyuan Xu, Qin Zhou, Qian Yu, Lu Sheng, and Dong Xu. Diffusion model is secretly a training-free open vocabulary semantic segmenter. *arXiv preprint arXiv:2309.02773*, 2023. [5](#)
- [33] Qixun Wang, Xu Bai, Haofan Wang, Zekui Qin, and Anthony Chen. Instantid: Zero-shot identity-preserving generation in seconds. *arXiv preprint arXiv:2401.07519*, 2024. [2](#), [3](#), [7](#)
- [34] Yibin Wang, Weizhong Zhang, Jianwei Zheng, and Cheng Jin. High-fidelity person-centric subject-to-image synthesis. In *CVPR*, pages 7675–7684, 2024. [2](#), [3](#), [6](#)
- [35] Yuxiang Wei, Yabo Zhang, Zhilong Ji, Jinfeng Bai, Lei Zhang, and Wangmeng Zuo. Elite: Encoding visual concepts into textual embeddings for customized text-to-image generation. *arXiv preprint arXiv:2302.13848*, 2023. [3](#)
- [36] Guangxuan Xiao, Tianwei Yin, William T Freeman, Frédo Durand, and Song Han. Fastcomposer: Tuning-free multi-subject image generation with localized attention. *arXiv preprint arXiv:2305.10431*, 2023. [3](#), [7](#)
- [37] Hu Ye, Jun Zhang, Sibao Liu, Xiao Han, and Wei Yang. Ip-adapter: Text compatible image prompt adapter for text-to-image diffusion models. *arXiv preprint arXiv:2308.06721*, 2023. [10](#)
- [38] Kaipeng Zhang, Zhanpeng Zhang, Zhifeng Li, and Yu Qiao. Joint face detection and alignment using multitask cascaded convolutional networks. *IEEE signal processing letters*, 23(10):1499–1503, 2016. [6](#)
- [39] Shilong Zhang, Lianghua Huang, Xi Chen, Yifei Zhang, Zhi-Fan Wu, Yutong Feng, Wei Wang, Yujun Shen, Yu Liu, and Ping Luo. Flashface: Human image personalization with high-fidelity identity preservation. *arXiv preprint arXiv:2403.17008*, 2024. [3](#), [7](#)

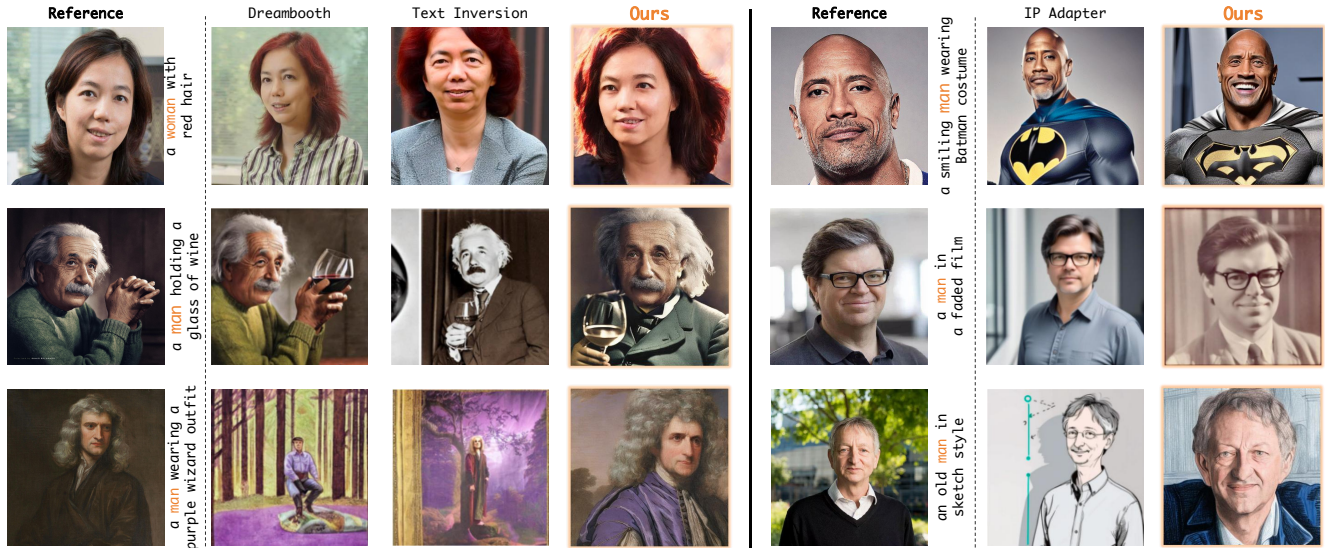


Figure 10. Qualitative comparative results on subject-to-image generation.

A. More compared baselines

We also compare our method with tuning-based baselines, i.e., Dreambooth [24] and Text Inversion [9], and a zero-shot baseline, IP-adapter [37]. The quantitative and qualitative results are provided in Tab. 2 and Fig. 10, respectively.

Table 2. Quantitative comparison against baselines.

Methods	Subject-to-Image Generation			
	CLIP-T	CLIP-I	DINO	Face-sim.
'23 Dreambooth (SDXL)	31.6	58.4	37.4	43.2
'23 Text Inversion (SD1.5)	26.7	63.1	36.9	48.6
'23 IP-adapter (SDXL)	27.3	64.9	47.5	62.8
MagicFace (SD1.5)	33.6	76.5	55.2	66.1

B. Inference Time Comparison

Our method is entirely training-free and personalizes a human image with just a single forward pass. We also compare inference times with selected efficient baselines using 50 steps of the DDIM sampler, as shown in Tab. 3.

C. User Study

We conduct user studies to make a more comprehensive comparison. Specifically, we invite 30 participants through voluntary participation and assign them the task of completing 40 ranking questions. Each question includes reference images, the corresponding text prompt, and the generated images of competitive methods. We anonymize the names of all methods and randomize the order of methods in each question. The ranking criteria comprehensively considered factors including ID Fidelity, Image Quality, and Prompt Consistency. We collect 23 valid questionnaires for subject-to-image generation and 26 for multi-concept customization.

Table 3. Inference time comparison. '-' indicates that the information is not available.

Methods	Fastcomposer	Photomaker	FreeCustom	Ours
single-concept	7s	12s	20s	10s
2-concept	-	-	36s	18s
3-concept	-	-	58s	25s

Table 4. User study on subject-to-image generation: higher score, better ranking.

Methods	ID Fidelity	Image Quality	Prompt Consistency
PhotoMaker	2.28	2.06	2.19
InstantID	2.07	2.23	2.21
FlashFace	2.64	2.59	2.32
Ours	3.01	3.12	3.28

The results are presented in Tab. 4 and Tab. 5. Notably, our method received favorable feedback from the majority of participants.

D. More visual results

More visual results generated by our method are shown in Fig. 12 and Fig. 13.

E. Choice of self-attention layer replacement

We explore the optimal choice of replacing the original self-attention in the basic block with our RSA/RBA, as shown in Fig. 16 and Fig. 17. The results indicate that replacing the self-attention layers in blocks 5 and 6 produces the highest fidelity images.

F. Choice of weight w

We provide more cases for exploring the impacts of different weight settings in Fig. 15.

Table 5. User study on multi-concept customization: higher score, better ranking.

Methods	ID Fidelity	Image Quality	Prompt Consistency
CustomDiffusion	1.56	1.94	1.83
FreeCustom	3.07	2.59	2.98
ClassDiffusion	1.83	2.07	2.03
Ours	3.54	3.40	3.16

G. Choice of hyperparameter α

We provide an additional case for exploring the optimal value of α as shown in Fig. 11.

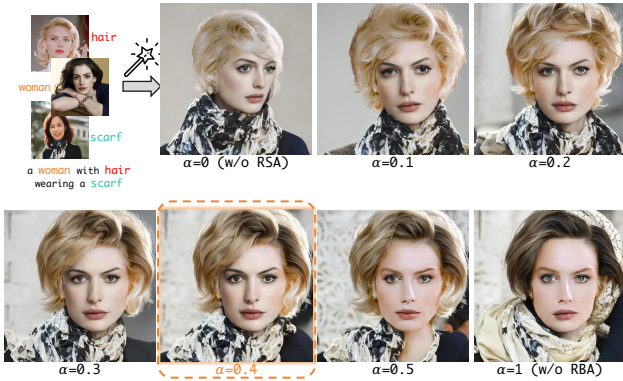


Figure 11. Hyperparameter analysis of α .

H. Visualizatoin of RSA and RBA

More visualization results of RSA and RBA are shown in Fig. 14.

I. Limitation

MagicFace is capable of synthesizing high-fidelity human images, which, while impressive, raises significant privacy and security concerns. This high level of fidelity can lead to the unauthorized use of personal face portraits, potentially resulting in ethical issues and hindering the broader adoption of such technology. Ensuring that these tools are used responsibly and with proper consent is crucial to mitigating these risks.

J. Societal impact

The societal impact of personalized human image generation technologies, such as MagicFace, is profound. These innovations drive creativity in entertainment, virtual reality, and augmented reality, enabling highly realistic content in video games and films that greatly enhance user experiences. However, as these technologies become increasingly accessible, they raise significant concerns about privacy, consent, and potential misuse. Balancing innovation with ethical

considerations is essential to fully realize the benefits of subject-driven text-to-image generation while safeguarding societal interests.

K. Superiority compared with baselines

Training-Free Approach. Existing human-centric subject-to-image generation methods typically rely on extensive retraining on large-scale datasets or fine-tuning with dozens of images. These approaches involve time-consuming processes, making rapid deployment challenging. In contrast, MagicFace is entirely training-free, eliminating the need for large-scale pre-training and the associated computational overhead. By requiring only a single image per concept, our approach is significantly more efficient and practical, reducing both time and computational resource demands. **High-fidelity Results.** Despite the simplicity, our method consistently delivers more natural and realistic human personalization results. Extensive quantitative and qualitative evaluations demonstrate that our approach matches or even surpasses the performance of more complex, training-based methods, highlighting its effectiveness in producing high-fidelity human images.

Versatility in Applications. (1) *Universal-style human customization.* Unlike existing methods constrained by their training datasets to only photorealistic styles, our method excels at customizing a wide range of styles. By accurately embedding reference concept features into the generated image in an evolving scheme, our method is adept at customized synthesizing images of humans across diverse styles. (2) *Texture transfer.* Our approach is not only superior in human image synthesis but also highly effective for texture transfer. By precisely extracting appearance features from input images and seamlessly integrating these features into generated objects, our method shows its robustness across different applications.

Multi-concept Human Customization. Compared to current human-centric subject-to-image generation methods which fail to personalize humans with multiple given concepts, our approach enables high-quality multi-concept human customization. For a more thorough evaluation, we also compare our method against specialized baselines in the multi-concept customization domain. While these methods handle general objects with coarse-grained textures reasonably well, our experimental results indicate that they falter in human-centric customization. In contrast, our approach precisely preserves human identity, setting a new benchmark for multi-concept human image synthesis.

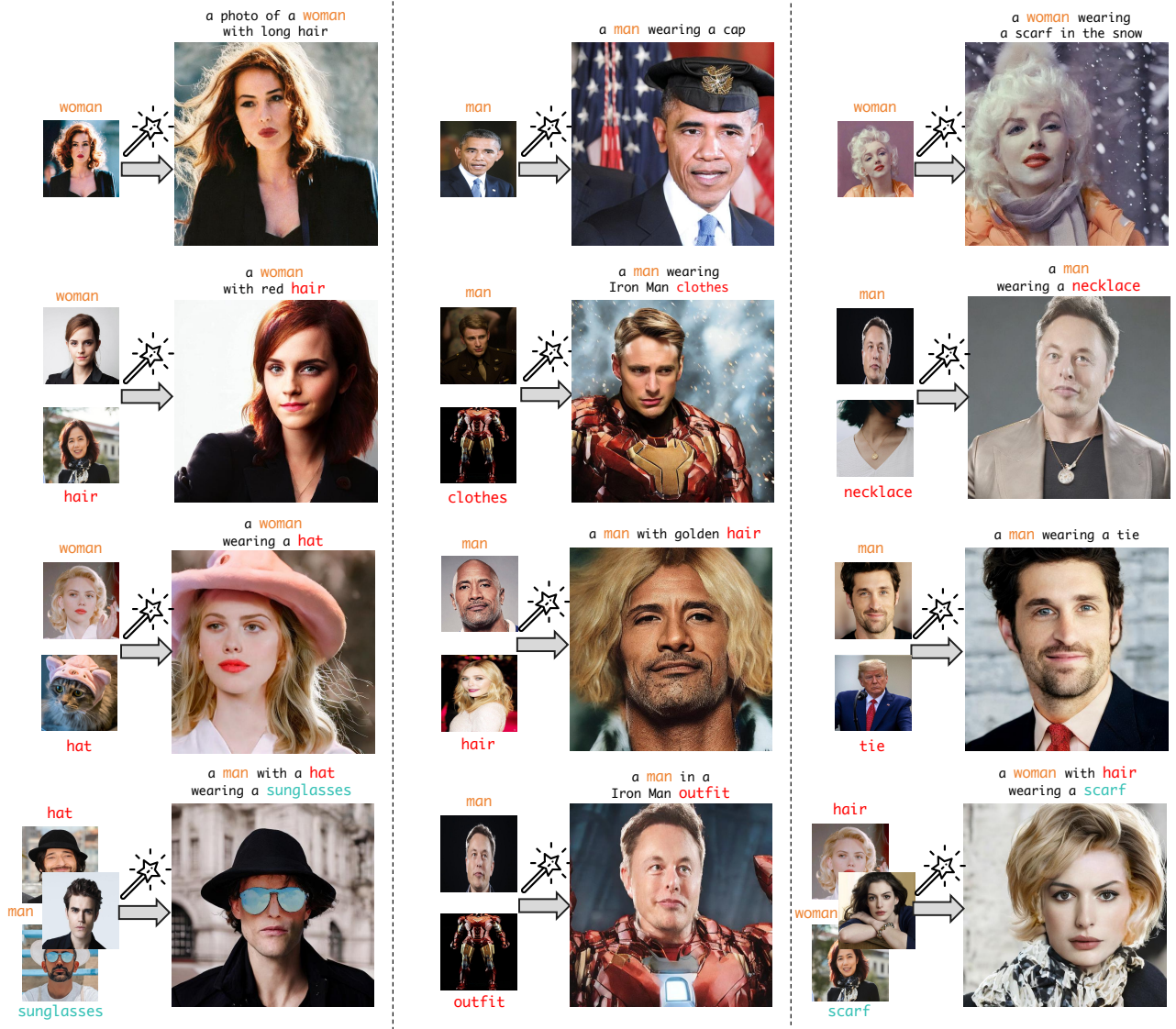


Figure 12. More visual results of single/multi-concept customization for humans of photorealism style.

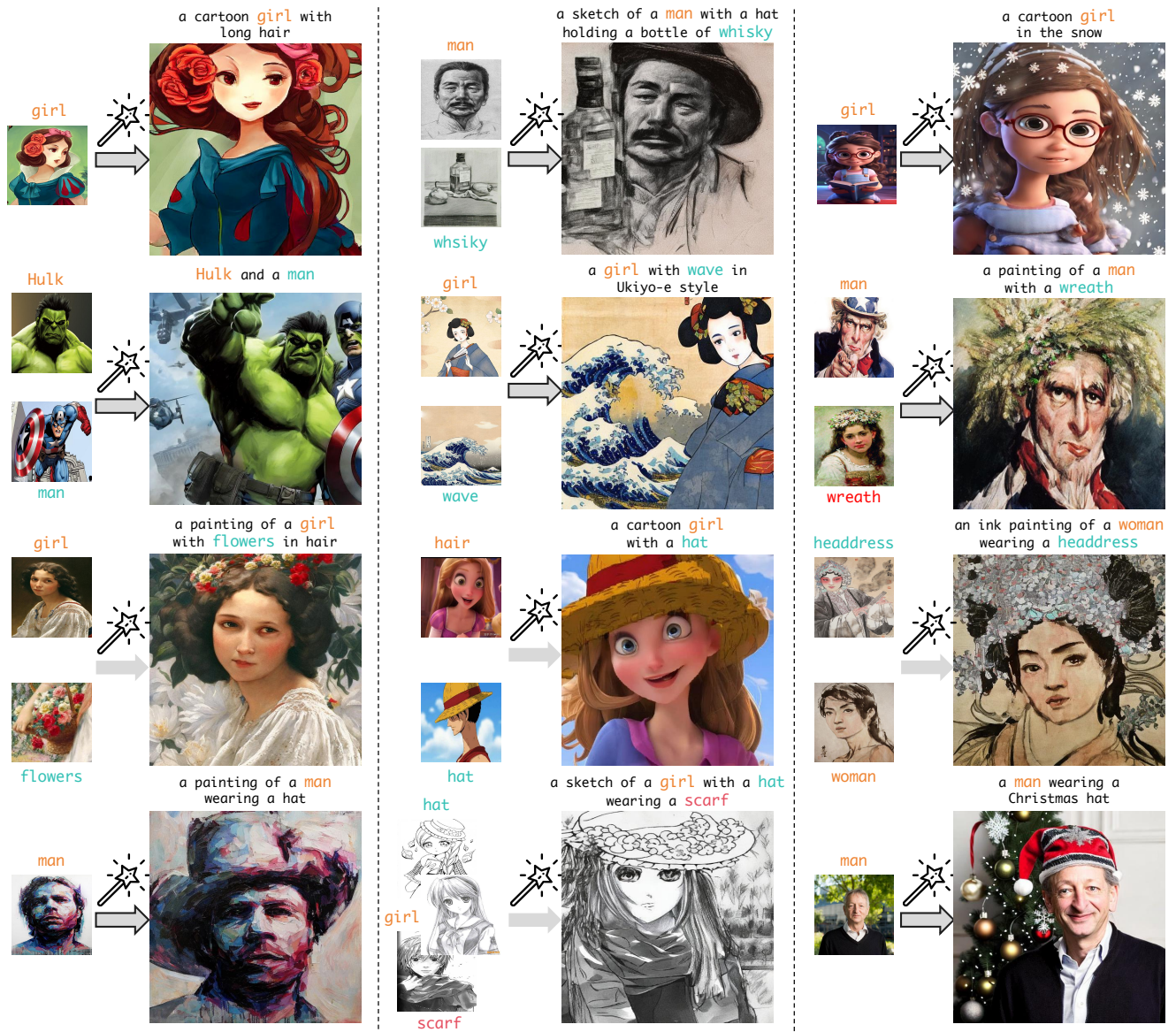


Figure 13. More visual results of single/multi-concept customization for humans of various styles.

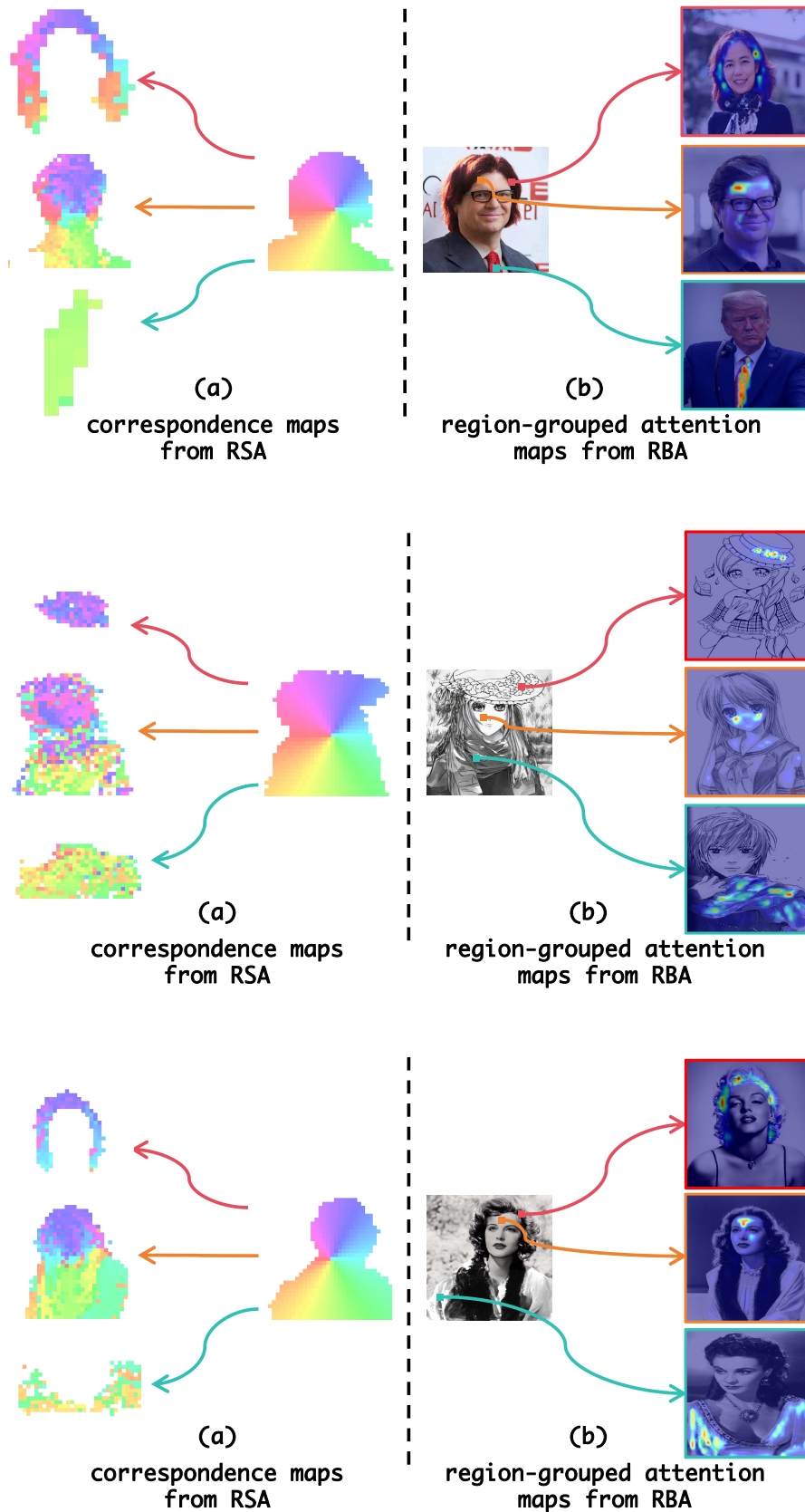


Figure 14. **Correspondence maps and region-grouped attention maps visualization.** In (a), features with the highest similarity between the generated subject and the reference concepts are marked with the same color. (b) the results of features in colored boxes querying their reference concept keys.

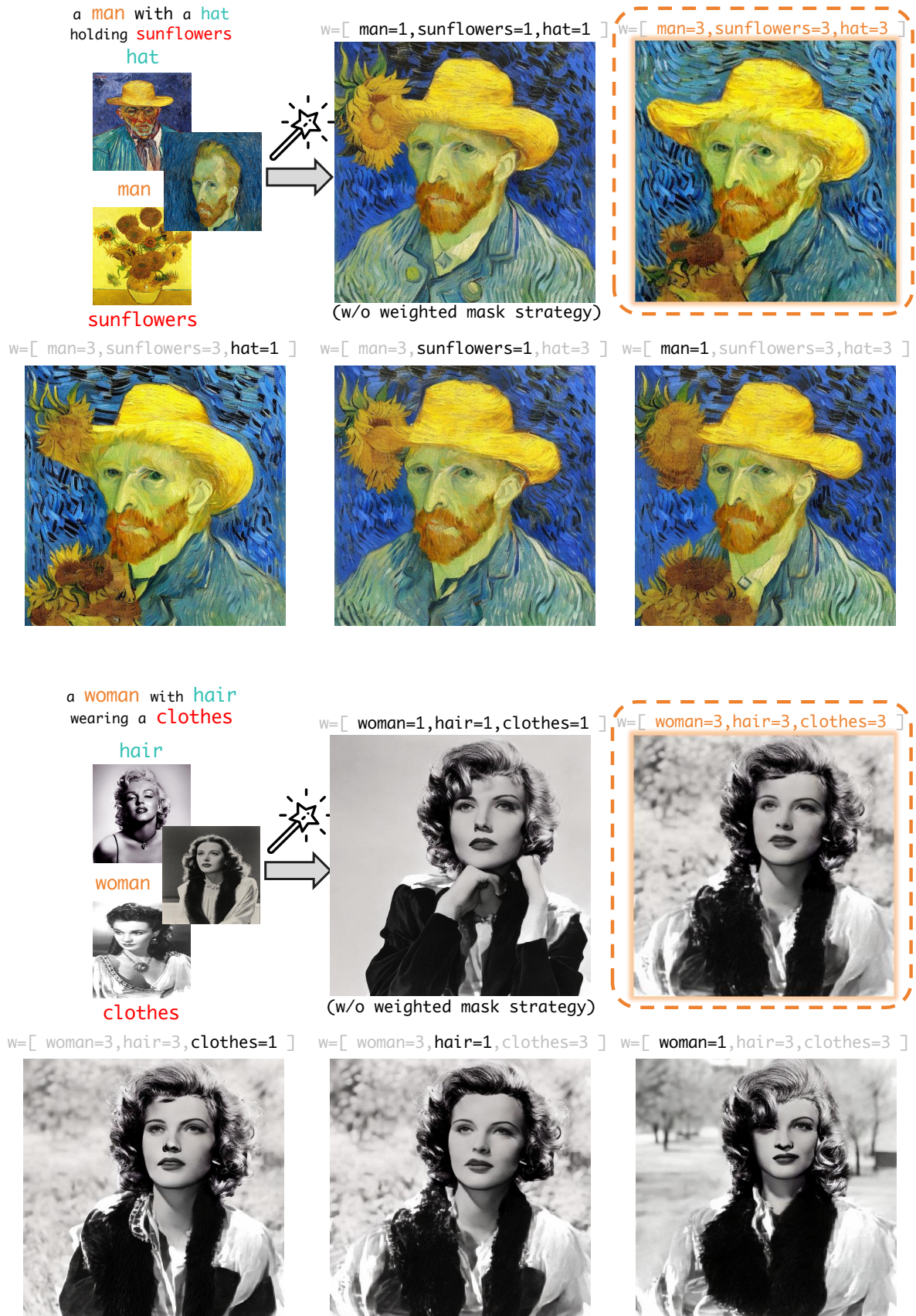


Figure 15. Visualized results under different weight settings w .

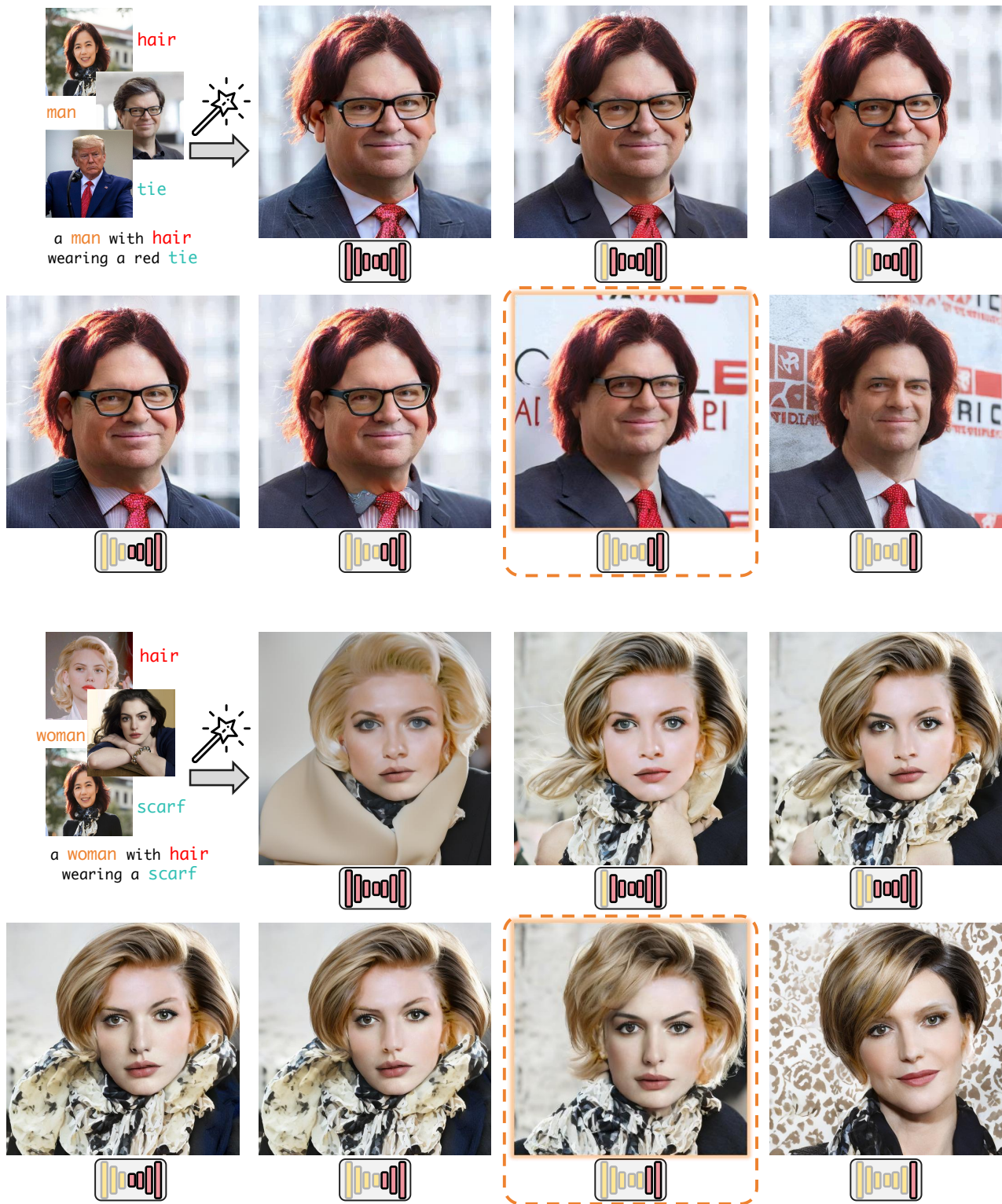


Figure 16. **Choice of self-attention layer replacement.** The yellow color represents the original basic block, while the red color indicates the basic block where the self-attention modules have been replaced by RSA/RBA.

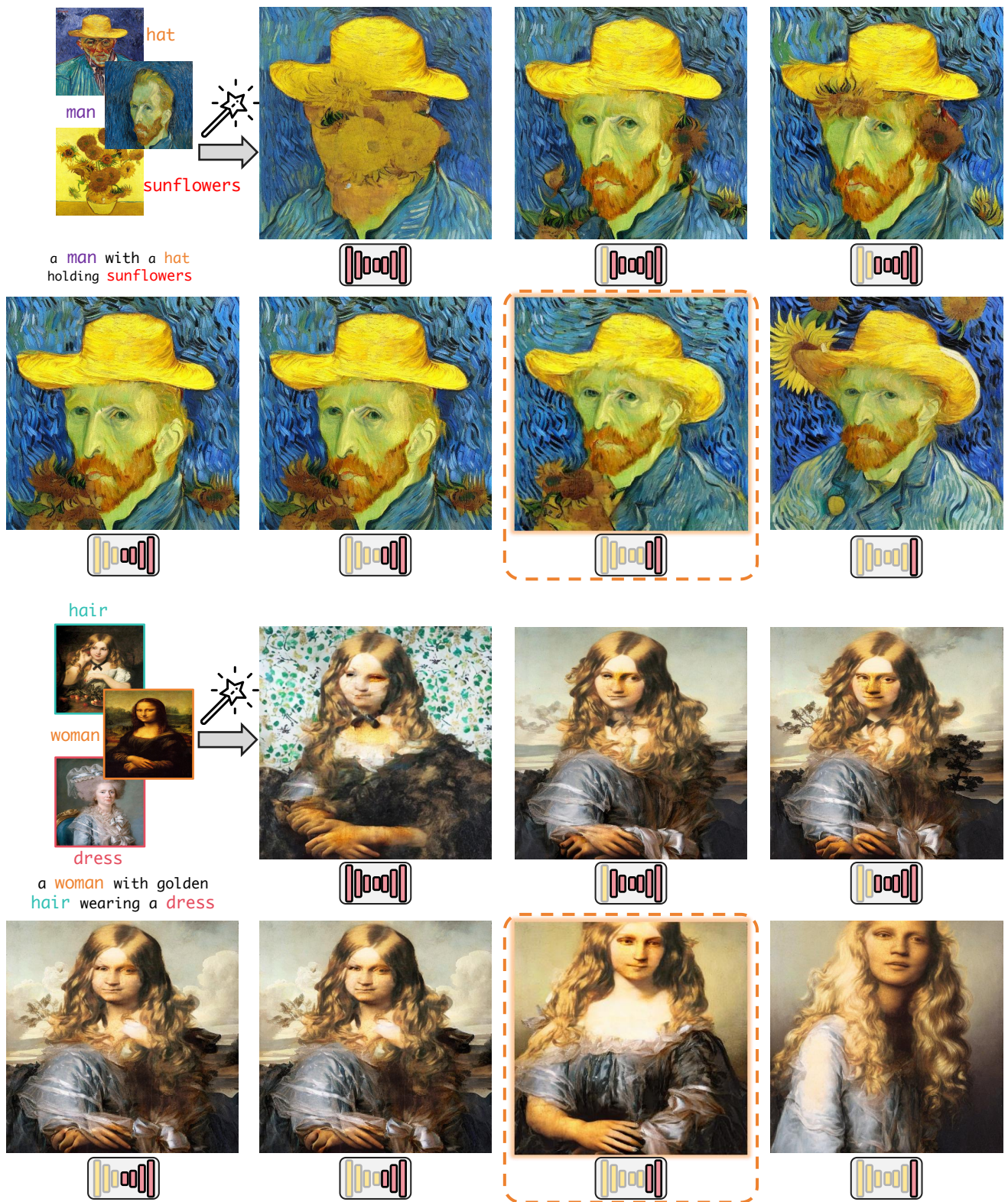


Figure 17. **Choice of self-attention layer replacement.** The yellow color represents the original basic block, while the red color indicates the basic block where the self-attention modules have been replaced by RSA/RBA.